

PREDEFINED-TIME AFFINE FORMATION FAULT-TOLERANT CONTROL FOR FIXED-WING UAVS WITH INPUT SATURATION

Fang Jun[1], Guo Yong[1], Li Aijun[1], Wang Changqing[1]

[1]School of Automation, Northwestern Polytechnical University, China

Abstract

A novel predefined-time fault-tolerant affine formation control law is proposed for fixed-wing unmanned aerial vehicles (UAVs) subject to input constraints and actuator faults. First, to address actuator fault issues, an input signal fault model is established. Considering the asymmetry of axial control inputs in UAVs, a smooth function is constructed to process the limited input signals, transforming the fault-tolerant and input-constrained control problems into a variable-gain control framework. Second, a predefined-time observer is employed to estimate external disturbances and the unknown dynamics induced by the variable-gain formulation. Based on the backstepping control framework, a predefined-time anti-saturation affine formation fault-tolerant control law is then developed. Finally, numerical simulations are conducted to verify that the proposed control law possesses strong disturbance rejection and anti-saturation capabilities, and can achieve fault-tolerant affine formation of UAVs within a predefined time.

Keywords: Affine Formation Control; Predefined-Time Control; Input Saturation; Fault-Tolerant Control

1. Introduction

In recent years, UAV formations have received significant attention in military and civilian applications owing to their high efficiency, safety, and operational flexibility [1][3]. Motivated by these advantages, numerous formation control strategies have been proposed for multi-UAV systems. Among them, affine formation control has emerged as a promising approach capable of achieving formation maneuvers including translation, rotation, and scaling. Due to its superior maneuverability and scalability, affine formation control has attracted increasing interest from researchers worldwide. The concept of affine formation was first introduced by the team led by Lin [4] at Zhejiang University, where the stability conditions of affine formations under both undirected and directed graphs were established. Building upon this work, Zhao [5] achieved affine formation control for both single-integrator and double-integrator systems under undirected graphs, and verified the feasibility of the proposed approach for both fixed and time-varying leader positions. Subsequently, extensive research efforts have been devoted to affine formation control, leading to significant developments in this field [6][8]. However, it is worth noting that these methods only guarantee asymptotic convergence and do not explicitly address the convergence rate.

To improve the convergence performance of affine formation control systems, considerable research efforts have been devoted to this topic. In recent years, finite-time control methods [9] have been widely applied to affine formation control due to their fast convergence, strong disturbance rejection capability, and high control accuracy. Although finite-time control can guarantee that the system states converge to the equilibrium point within a finite time, the upper bound of the convergence time may increase significantly and even become difficult to predict when the initial conditions are large or uncertainties are present. To address this issue, fixed-time control methods [10] were developed, which provide an upper bound on the convergence time independent of the initial conditions. However, the estimation of this upper bound usually requires complicated calculations. More recently, predefined-time affine formation control methods [11] have attracted considerable attention because the upper bound of the settling time can be directly specified by a single design parameter and is independent of both the controller parameters and the initial system states. This feature greatly facilitates practical engineering implementation and has made predefined-time control a popular research topic. In addition, during mission execution, actuator faults may occur in UAVs. Once a fault appears, the resulting tracking errors can propagate through the communication network, potentially degrading the formation performance and even causing instability of the entire UAV team. Consequently, ensuring robustness, reliability, and safety in the presence of faults has become a critical challenge for multi-UAV affine formation control systems.

Fault-tolerant control has been widely adopted in cooperative affine formation control as an effective means of enhancing system robustness. It can maintain the tracking errors within an acceptable range even when faults occur. Wang et al. [12] investigated the fault-tolerant affine formation control problem for multi-agent systems subject to loss-of-effectiveness and bias actuator faults. However, most existing studies on fault-tolerant affine formation control have focused on generic multi-agent systems, while relatively little attention has been devoted to UAV affine formation systems. The unique dynamics, stringent performance requirements, and safety considerations of UAV formations make the fault-tolerant affine formation control problem considerably more challenging. Meanwhile, practical actuators are inherently subject to physical limitations, which impose constraints on the control inputs. Consequently, the issue of input constraints has become another important research topic in the field of nonlinear control.

Considerable progress has been made in addressing input magnitude constraints. One widely adopted approach is to transform the input saturation problem into a variable-gain control problem by employing the mean value theorem. In this framework, smooth functions such as the Gaussian error function [13] and hyperbolic tangent function [14] are utilized to approximate the saturation nonlinearity, and anti-saturation control is subsequently achieved by incorporating adaptive techniques [15] or Nussbaum-type functions [16]. Another common approach is to design auxiliary systems to compensate for the discrepancy between the desired control inputs and the actual saturated inputs [17]. However, the aforementioned anti-saturation control methods mainly focus on symmetric input saturation problems. In contrast, fixed-wing UAVs cannot hover like quadrotor UAVs, and their axial control inputs must remain strictly positive, resulting in inherently asymmetric input

constraints. This characteristic poses additional challenges to the design of anti-saturation affine formation control strategies and demands more sophisticated control schemes.

To address the aforementioned challenges and meet the demand for rapid and flexible adaptation of UAV formations to environmental changes during mission execution, this paper investigates the predefined-time affine formation control problem for UAV systems subject to actuator faults, input constraints, and external disturbances. The main contributions of this paper are summarized as follows:

1) A predefined-time affine formation control strategy is developed to achieve affine maneuvers, including translation, scaling, and shearing, while guaranteeing that the UAV states converge to a prescribed neighborhood within a predefined time.

2) A novel smooth-function-based transformation is proposed to handle asymmetric input constraints. By utilizing the proposed smooth function, the fault-tolerant control problem under input constraints is transformed into a variable-gain control problem, which facilitates the subsequent controller design.

3) An observer-based predefined-time adaptive affine formation controller is developed to simultaneously compensate for actuator faults and handle asymmetric input constraints, thereby guaranteeing predefined-time convergence and improving system robustness.

2. Preliminaries

In this section, we will introduce the basic notations for the formations and leader-follower structure in affine formation. Then the research problem will be formulated.

In this paper, $\|\cdot\|$ indicates the Euclidean norm. $\mathbb{R}^{a\times b}$ indicates the set of $a\times b$ dimensional matrices. $\mathbb{R}^{a}$ indicates the set of a dimensional vectors. $\mathbb{R}$ indicates the set of real numbers. $\boldsymbol{I}_N$ denotes the $N\times N$ identity matrix, $\boldsymbol{1}_N$ indicates the N-dimensional column vector with all elements equal to 1, and $\otimes$ denotes the Kronecker product. $[\cdot]_i$ indicates the i-th row of the matrix.

2.1 Graph Theory

Consider a leader-follower UAV formation system consisting of N UAVs in $\mathbb{R}^d$ with $d\geq 2$ and $N\geq d+1$, in which $\boldsymbol{p}_i=[x_i,y_i,z_i]^{\mathrm{T}}\in\mathbb{R}^d$ denotes the position of UAV i and $\boldsymbol{p}=\left[\boldsymbol{p}_1^{\mathrm{T}},\boldsymbol{p}_2^{\mathrm{T}},\ldots,\boldsymbol{p}_N^{\mathrm{T}}\right]^{\mathrm{T}}\in\mathbb{R}^{dN}$ is the configuration of all the UAVs. Without loss of generality, assume that the formation system contains N_l leaders, where the configurations of the leaders and followers are denoted by $\boldsymbol{p}_l=\left[\boldsymbol{p}_1^{\mathrm{T}},\boldsymbol{p}_2^{\mathrm{T}},\ldots,\boldsymbol{p}_{N_l}^{\mathrm{T}}\right]^{\mathrm{T}}$ and $\boldsymbol{p}_f=\left[\boldsymbol{p}_{N_l+1}^{\mathrm{T}},\boldsymbol{p}_{N_l+2}^{\mathrm{T}},\ldots,\boldsymbol{p}_N^{\mathrm{T}}\right]^{\mathrm{T}}$, respectively, such that $\boldsymbol{p}=\left[\boldsymbol{p}_l^{\mathrm{T}},\boldsymbol{p}_f^{\mathrm{T}}\right]^{\mathrm{T}}$.

The communication topology among the UAVs can be described by an undirected graph $G=(\upsilon,\varepsilon)$, where $\upsilon=\{\upsilon_1,\ldots,\upsilon_N\}$ is the set of vertices and $\varepsilon\subseteq\upsilon\times\upsilon$ is the set of edges. An edge $(i,j)\in\varepsilon$ indicates that vertex υ_i can obtain information from vertex υ_j. The neighbor set of vertex υ_i are denoted by $N_i=\{j\in\upsilon:(i,j)\in\varepsilon\}$.

2.2 Affine Formation

An affine formation transformation is a standard linear transformation that encompasses translation, rotation, scaling, and shearing, as well as any combination of these operations. Denote $(G,\boldsymbol{p})$ as the one-to-one mapping between the i-th UAV and vertex υ_i in the graph. The nominal formation of graph G can be represented by $(G,\boldsymbol{r})$, where $\boldsymbol{r}=\left[\boldsymbol{r}_1^{\mathrm{T}},\boldsymbol{r}_2^{\mathrm{T}},\ldots,\boldsymbol{r}_N^{\mathrm{T}}\right]^{\mathrm{T}}\in\mathbb{R}^{dN}$ is a constant matrix denoting the nominal configuration. The affine mapping of the nominal configuration under an affine transformation can be expressed as:

$$A(\boldsymbol{r})=\left\{\boldsymbol{p}\in\mathbb{R}^{dN}:\boldsymbol{p}=(\boldsymbol{I}_N\otimes A)\boldsymbol{r}+\boldsymbol{1}_N\otimes\boldsymbol{b}\right\} \tag{1}$$

where $A(\boldsymbol{r})$ denotes the set of all affine transformations of the nominal configuration $\boldsymbol{r}$. $\boldsymbol{A}\in\mathbb{R}^{d\times d}$ and $\boldsymbol{b}\in\mathbb{R}^{d}$ are from the corresponding affine transformation. Given a set of positions $\{\boldsymbol{p}_i\}_{i=1}^N$, the affine span of this set, denoted as S, can be expressed as:

$$S=\left\{\sum_{i=1}^{n}a_i\boldsymbol{p}_i:a_i\in\mathbb{R}\ \text{for all}\ i\ \text{and}\ \sum_{i=1}^{n}a_i=1\right\} \tag{2}$$

Then, the target formation with maneuvers can be described by

$$\boldsymbol{p}^{*}(t)=\left[\boldsymbol{I}_{N}\otimes A(t)\right]\boldsymbol{r}+\boldsymbol{1}_{N}\otimes\boldsymbol{b}(t) \tag{3}$$

where $\boldsymbol{b}(t)\in\mathbb{R}^{d}$ represents the formation's translational maneuver, and $A(t)\in\mathbb{R}^{d\times d}$ can be used to realize the whole formation's rotational, scaling, and shearing maneuvers with respect to the nominal configuration $\boldsymbol{r}$. Thus, the desired position of the i-th UAV in the target formation is

$$\boldsymbol{p}_{i}^{*}(t)=A(t)\boldsymbol{r}_{i}+\boldsymbol{b}(t) \tag{4}$$

To further characterize the interactions among UAVs, the concept of the signed Laplacian is introduced. The signed Laplacian matrix, also referred to as the stress matrix, is defined by assigning a scalar weight ω_{ij}, $(i,j)\in\varepsilon$ to each edge in $(G,\boldsymbol{p})$. The collection of these weights is called the stress. For an undirected graph, it holds that $\omega_{ij}=\omega_{ji}$. A positive weight $\omega_{ij}>0$ indicates an attractive interaction along edge (i,j) whereas a negative weight $\omega_{ij}<0$ indicates a repulsive interaction. The resultant force acting on the i-th UAV can be expressed as $\sum_{j\in N_i}\omega_{ij}(p_j-p_i)$. When all the forces acting on the UAVs are balanced, the corresponding set of scalar weights is referred to as a self-stress, i.e., $\sum_{j\in N_i}\omega_{ij}(\boldsymbol{p}_j-\boldsymbol{p}_i)=0$.The above equation can be further rewritten in matrix form as:

$$\left(\Omega\otimes\boldsymbol{I}_{d}\right)\boldsymbol{p}=0 \tag{5}$$

where $\boldsymbol{\Omega}\in\mathbb{R}^{N\times N}$ denotes the stress matrix, which can be expressed as follows:

$$\left[\boldsymbol{\Omega}\right]_{ij}=\begin{cases}0, & i\neq j,(i,j)\notin\varepsilon\\ -\omega_{ij}, & i\neq j,(i,j)\in\varepsilon\\ \sum_{k\in N_i}\omega_{ik}, & i=j\end{cases} \tag{6}$$

In this paper, an affine formation maneuver control strategy based on the leader-follower architecture is adopted. For simplicity, define $\bar{\boldsymbol{\Omega}}=\boldsymbol{\Omega}\otimes\boldsymbol{I}_{d}$ as follows:

$$\bar{\boldsymbol{\Omega}}=\boldsymbol{\Omega}\otimes\boldsymbol{I}_{d}=\begin{bmatrix}\boldsymbol{\Omega}_{ll} & \boldsymbol{\Omega}_{lf}\\ \boldsymbol{\Omega}_{fl} & \boldsymbol{\Omega}_{ff}\end{bmatrix}\otimes\boldsymbol{I}_{d}=\begin{bmatrix}\bar{\boldsymbol{\Omega}}_{ll} & \bar{\boldsymbol{\Omega}}_{lf}\\ \bar{\boldsymbol{\Omega}}_{fl} & \bar{\boldsymbol{\Omega}}_{ff}\end{bmatrix} \tag{7}$$

2.3 UAV Dynamic Model with External Disturbances and Faults

The model of fixed-wing UAV with external disturbances is introduced as:

$$\begin{cases}\dot{x}_i=V_i\cos\gamma_i\cos\chi_i\\ \dot{y}_i=V_i\cos\gamma_i\sin\chi_i\\ \dot{z}_i=-V_i\sin\gamma_i\end{cases} \tag{8}$$

$$\begin{cases}\dot{V}_i=\dfrac{T_i-D_i+d_{Vi}}{m_i}-g\sin\gamma_i\\ \dot{\chi}_i=\dfrac{L_i\sin\phi_i+d_{\chi i}}{m_iV_i\cos\gamma_i}\\ \dot{\gamma}_i=\dfrac{L_i\cos\phi_i-m_ig\cos\gamma_i+d_{\gamma i}}{m_iV_i}\end{cases} \tag{9}$$

where x_i, y_i, and z_i are the coordinates of i-th UAV, m_i is the mass, V_i is the velocity. ϕ_i, γ_i, and χ_i are the bank angle, flight path angle, and heading angle. T_i, L_i, and D_i are the thrust, lift, and drag. g is the acceleration due to gravity. d_{Vi}, $d_{\gamma i}$, and $d_{\chi i}$ are the bounded disturbances. To simplify the derivation, the vector form of the UAV model can be used as:

$$\begin{cases}\dot{\boldsymbol{p}}_{i1}=\boldsymbol{p}_{i2}\\ \dot{\boldsymbol{p}}_{i2}=\dfrac{\boldsymbol{R}_i}{m_i}\boldsymbol{u}_{if}+\boldsymbol{\alpha}_i+\boldsymbol{d}_i\end{cases} \tag{10}$$

where $\boldsymbol{p}_{i1}=\left[x_i,y_i,z_i\right]^{\mathrm{T}}$ and $\boldsymbol{p}_{i2}=\left[\dot{x}_i,\dot{y}_i,\dot{z}_i\right]^{\mathrm{T}}$ are the position and velocity of the *i*-th UAV. $\boldsymbol{u}_i=\left[T_i,L_i\,sin\phi_i,-L_i\,cos\phi_i\right]^{\mathrm{T}}$ is the input signal, $\boldsymbol{d}_i=\boldsymbol{R}_i\boldsymbol{d}_{i0}/m_i$ is the disturbances for $\boldsymbol{d}_{i0}=\left[d_{Vi},d_{\gamma i},d_{\chi i}\right]^{\mathrm{T}}$, $\boldsymbol{\alpha}_i=\left[-D_i\,cos\gamma_i\,cos\chi_i,-D_i\,cos\gamma_i\,sin\chi_i,D_i\,sin\gamma_i+m_ig\right]/m_i$ is an intermediate variable, m_i is the mass, ϕ_i, γ_i, and χ_i are the bank angle, flight path angle, and heading angle. T_i, L_i, and D_i are the trust, lift, and drag. g is the acceleration due to gravity. d_{Vi}, $d_{\gamma i}$, and $d_{\chi i}$ are the bounded disturbances, and

$$\boldsymbol{R}_i=\begin{bmatrix}cos\gamma_i\,cos\chi_i & -sin\chi_i & sin\gamma_i\,cos\chi_i\\ cos\gamma_i\,sin\chi_i & cos\chi_i & sin\gamma_i\,sin\chi_i\\ -sin\gamma_i & 0 & cos\gamma_i\end{bmatrix} \tag{11}$$

where $\left\|\boldsymbol{R}_i\right\|=1$. Then, considering actuator faults, the input signal of the UAV can be expressed as follows:

$$\boldsymbol{u}_{if}=\varsigma_i\boldsymbol{u}_i+\boldsymbol{h}_{if} \tag{12}$$

where $\boldsymbol{h}_{if}\in\mathbb{R}^3$ is the unknown bias faults, $\varsigma_i=\mathrm{diag}\left\{\varsigma_{i1},\varsigma_{i2},\varsigma_{i3}\right\}$ is the fault indicators for $\varsigma_{ij}\in(0,1]$ and $j\in\{1,2,3\}$. $\boldsymbol{u}_i\in\mathbb{R}^3$ is the limited input signal.

Meanwhile, a constrained input signal can be expressed as

$$\boldsymbol{u}_i[j]=sat(\tilde{\boldsymbol{v}}_i[j])=\begin{cases}\bar{u} & if\ \tilde{\boldsymbol{v}}_i[j]>\bar{u}\\ \tilde{\boldsymbol{v}}_i[j] & if\ \underline{u}\le\tilde{\boldsymbol{v}}_i[j]\le\bar{u}\\ \underline{u} & if\ \tilde{\boldsymbol{v}}_i[j]<\underline{u}\end{cases} \tag{13}$$

To handle asymmetric input saturation, a novel smooth function based on the Gaussian error function $G(x)=\frac{2}{\sqrt{\pi}}\int_0^x e^{-t^2}dt$ is designed to approximate the constrained input function:

$$\mathrm{g}(\tilde{\boldsymbol{v}}_i[j])=u_M(\tilde{\boldsymbol{v}}_i[j])G(\frac{\sqrt{\pi}}{2u_M(\tilde{\boldsymbol{v}}_i[j])}\tilde{\boldsymbol{v}}_i[j]) \tag{14}$$

Where $u_M(\tilde{\boldsymbol{v}}_i[j])=(\bar{u}+\underline{u})/2+sign(\tilde{\boldsymbol{v}}_i[j])(\bar{u}-\underline{u})/2$. The constrained control input can then be expressed as $\boldsymbol{u}_i[j]=sat(\tilde{\boldsymbol{v}}_i[j])=\mathrm{g}(\tilde{\boldsymbol{v}}_i[j])+\rho(\tilde{\boldsymbol{v}}_i[j])$, where $\rho(\tilde{\boldsymbol{v}}_i[j])$ denotes the transformation error. According to the mean value theorem, there exists a scalar $v_\delta\in(\tilde{\boldsymbol{v}}_i[j]^*,\tilde{\boldsymbol{v}}_i[j])$ such that

$$\mathrm{g}(\tilde{\boldsymbol{v}}_i[j])=g(\tilde{\boldsymbol{v}}_i[j]^*)+\left.\frac{\partial g}{\partial\tilde{\boldsymbol{v}}_i[j]}\right|_{\tilde{\boldsymbol{v}}_i[j]=v_\delta}(\tilde{\boldsymbol{v}}_i[j]-\tilde{\boldsymbol{v}}_i[j]^*) \tag{15}$$

where $v_\delta=(1-\lambda)\tilde{\boldsymbol{v}}_i[j]^*+\lambda\tilde{\boldsymbol{v}}_i[j]$ and $\lambda\in(0,1)$. By defining $\tilde{\boldsymbol{v}}_i[j]^*=0$, (15) can be rewritten as

$$\mathrm{g}(\tilde{\boldsymbol{v}}_i[j])=\left.\frac{\partial g}{\partial\tilde{\boldsymbol{v}}_i[j]}\right|_{\tilde{\boldsymbol{v}}_i[j]=v_\delta}\tilde{\boldsymbol{v}}_i[j] \tag{16}$$

where $r_i\triangleq\left.\frac{\partial g}{\partial\tilde{\boldsymbol{v}}_i[j]}\right|_{\tilde{\boldsymbol{v}}_i[j]=v_\delta}$ denotes the value of the partial derivative of the function $\mathrm{g}(\tilde{\boldsymbol{v}}_i[j])$ with respect to $\tilde{\boldsymbol{v}}_i[j]$ evaluated at $\tilde{\boldsymbol{v}}_i[j]=v_\delta$, which satisfies

$$\begin{aligned}\mathrm{g}(\tilde{\boldsymbol{v}}_i[j])&=r_i\tilde{\boldsymbol{v}}_i[j]\\ &=exp(-(\frac{\sqrt{\pi}}{2u_M(\tilde{v}_i[j])}\tilde{\boldsymbol{v}}_i[j])^2)\Big|_{\tilde{\boldsymbol{v}}_i[j]=v_\delta}\tilde{\boldsymbol{v}}_i[j]\end{aligned} \tag{17}$$

Then, by considering actuator faults and input saturation, the mean value theorem is applied to reformulate the saturated input, such that the input signal of the UAV can be expressed as:

$$\begin{cases}\dot{\boldsymbol{p}}_{i1}=\boldsymbol{p}_{i2}\\ \dot{\boldsymbol{p}}_{i2}=\dfrac{\boldsymbol{R}_i}{m_i}\varsigma_i\sigma\tilde{v}_i+\boldsymbol{\Delta}_i+\boldsymbol{\alpha}_i\end{cases} \tag{18}$$

where $\Delta_i = \frac{\boldsymbol{R}_i}{m_i}\varsigma_i(r_i-\sigma)\tilde{v}_i + \frac{\boldsymbol{R}_i}{m_i}\varsigma_i\rho(\tilde{v}_i)+\boldsymbol{d}_i + \frac{\boldsymbol{R}_i}{m_i}\boldsymbol{h}_i$, σ is a given positive constant satisfying $0<\sigma_m\le\sigma\le 1$. $|\rho(\tilde{\boldsymbol{v}}_i)| = |sat(\tilde{\boldsymbol{v}}_i[j]) - g(\tilde{\boldsymbol{v}}_i[j])| \le |sat(\tilde{\boldsymbol{v}}_i[j])| + |g(\tilde{\boldsymbol{v}}_i[j])|$ is a bounded quantity satisfying $|\rho(\tilde{\boldsymbol{v}}_i)| \le |sat(\tilde{\boldsymbol{v}}_i[j])| + |g(\tilde{\boldsymbol{v}}_i[j])| = \bar{\rho}$, where $\bar{\rho}$ is a positive constant.

2.4 Key Assumptions and Lemmas

In this subsection, we present the theoretical preliminaries, including key assumptions and lemmas, related to affine formation and predefined-time convergence.

Assumption 1 [8]: For the nominal formation $(G,\boldsymbol{r})$, assume $\{\boldsymbol{r}_i\}_{i=1}^N$ affinely span $\mathbb{R}^d$.

Assumption 2 [8]: Assume that the nominal formation $(G,\boldsymbol{r})$ has a positive semi-definite stress matrix $\boldsymbol{\Omega}$ satisfying $rank(\boldsymbol{\Omega}) = N-d-1$.

Definition 1 [8]: The nominal formation $(G,\boldsymbol{r})$ is affinely localizable by the leaders if for any $\boldsymbol{p} = \left[\boldsymbol{p}_l^{\mathrm{T}}, \boldsymbol{p}_f^{\mathrm{T}}\right]^{\mathrm{T}} \in A(\boldsymbol{r})$, $\boldsymbol{p}_f$ can be uniquely determined by $\boldsymbol{p}_l$.

Assumption 3 [8]: The nominal formation $(G,\boldsymbol{r})$ is affinely localizable by the leaders.

Lemma 1 [8]: If Assumptions 1-3 hold, then

1) $\bar{\boldsymbol{\Omega}}_{ff}$ is positive definite;

2) for any $\boldsymbol{p} = \left[\boldsymbol{p}_l^{\mathrm{T}}, \boldsymbol{p}_f^{\mathrm{T}}\right]^{\mathrm{T}} \in A(\boldsymbol{r})$, $\boldsymbol{p}_f$ can be uniquely calculated as $\boldsymbol{p}_f = -\bar{\boldsymbol{\Omega}}_{ff}^{-1}\bar{\boldsymbol{\Omega}}_{fl}\boldsymbol{p}_l$.

Lemma 2 [18]: Considering a system like $\dot{x} = f(t,x)$, if there exists a candidate Lyapunov function $V(x)$, satisfying:

$$\dot{V} \le -\frac{1}{pT_c}exp(\beta V^p)V^{1-p} + \hat{\lambda} \tag{19}$$

where $T_c > 0$; $0 < p \le 1$ are constants, and $0 < \hat{\lambda} < \infty$ is a bounded normal constant, then for any initial state, the system states converge to the set $\Omega = min\{\Omega_1, \Omega_2\}$ within the predefined time $t = max\{t_1, t_2\}$, where

$$\begin{cases} t_1 = \frac{T_c}{\alpha\beta}(1-exp(-\beta V_0^p)) < \frac{T_c}{\alpha\beta} \\ t_2 = \frac{T_c}{(1-\alpha)\beta}(1-exp(-\beta V_0^p)) < \frac{T_c}{(1-\alpha)\beta} \end{cases} \tag{20}$$

$$\begin{cases} \Omega_1 = \left\{ x \middle| exp(\beta V^p)V^{1-p} \le \frac{\hat{\lambda} pT_c}{1-\alpha} \right\} \\ \Omega_2 = \left\{ x \middle| exp(\beta V^p)V^{1-p} \le \frac{\hat{\lambda} pT_c}{\alpha} \right\} \end{cases} \tag{21}$$

Lemma 3 [18]: Considering a system like $\dot{x} = f(t,x)$, if there exists a candidate Lyapunov function $V(x)$, satisfying:

$$\dot{V} \le -\frac{1}{pT_c}exp(\beta V^p)V^{1-p} \tag{22}$$

where $T_c > 0$; $0 < p \le 1$ are constants, then for any initial state. Then the system is predefined-time stable with the predefined-time T_c.

Lemma 4 [19]: For any bounded smooth function $\varepsilon > 0$, $z \in \mathbb{R}$, the following inequality holds:

$$0 \le |z| - \frac{z^2}{\sqrt{z^2 + \varepsilon^2}} < \varepsilon \tag{23}$$

Lemma 5 [20]: If $a_1 > 0$, $a_2 > 0$, $a_3 > 0$, and $0 < \breve{\gamma} \le 1$, then we have:

$$exp(a_3 a_1^{\breve{\gamma}}) a_1^{1-\breve{\gamma}} + exp(a_3 a_2^{\breve{\gamma}}) a_2^{1-\breve{\gamma}} \ge \frac{1}{2}\left[exp(a_3 a_1^{\breve{\gamma}}) + exp(a_3 a_2^{\breve{\gamma}})\right]\left[a_1^{1-\breve{\gamma}} + a_2^{1-\breve{\gamma}}\right] \tag{24}$$

Lemma 6 [20]: If $a_1 > 0$, $a_2 > 0$, and $0 < \breve{\gamma} \le 1$, we have:

$$a_1^{\breve{\gamma}} + a_2^{\breve{\gamma}} \ge (a_1 + a_2)^{\breve{\gamma}} \tag{25}$$

3. Controller design

In this subsection, the controller design procedure is presented. Since the control architecture is distributed, each UAV can only get information from its neighbors. Accordingly, the error system is defined as follows:

$$\boldsymbol{e}_{ip} = \boldsymbol{p}_i(t) - \boldsymbol{p}_i^*(t) \tag{26}$$

$$\boldsymbol{e}_{iv} = \dot{\boldsymbol{p}}_i(t) - \dot{\boldsymbol{p}}_{id}(t) \tag{27}$$

where $\boldsymbol{e}_{ip}$ and $\boldsymbol{e}_{iv}$, are the position error and velocity error. $\boldsymbol{p}_i^*(t) = -\left[\bar{\Omega}_{ff}^{-1}\bar{\Omega}_{fl}\right]^i \boldsymbol{p}_l^*(t)$ represents the desired position of the i-th follower. Owing to the continuity and boundedness of the leaders' states, it is assumed without loss of generality that $\left|\boldsymbol{p}_i^*(t)\right| \le \bar{P}$, where $\bar{P}$ is an unknown positive constant.

3.1 Observer Design

To estimate Δ_i accurately and quickly, a predefined-time observer is constructed as follows:

$$\hat{\Delta}_i = \varepsilon \hat{\boldsymbol{e}}_\Delta + \dot{\boldsymbol{e}}_\Delta \tag{28}$$

$$\dot{\hat{\boldsymbol{p}}}_{i2} = \frac{\boldsymbol{R}_i}{m_i}\varsigma_i \sigma \tilde{\boldsymbol{v}}_i + \boldsymbol{\alpha}_i + \varepsilon \boldsymbol{e}_\Delta \tag{29}$$

$$\dot{\hat{\boldsymbol{e}}}_\Delta = \dot{\boldsymbol{e}}_\Delta + \frac{1}{T_{c1}}\Phi(\tilde{\boldsymbol{e}}_\Delta) \tag{30}$$

where, $\hat{\Delta}_i$, $\hat{\boldsymbol{e}}_\Delta$, and $\hat{\boldsymbol{p}}_{i2}$ are the estimate signals of Δ_i, $\boldsymbol{e}_\Delta$, and $\boldsymbol{p}_{i2}$ respectively. $\boldsymbol{e}_\Delta = \boldsymbol{p}_{i2} - \hat{\boldsymbol{p}}_{i2}$, $\tilde{\boldsymbol{e}}_\Delta = \boldsymbol{e}_\Delta - \hat{\boldsymbol{e}}_\Delta$, $\Phi(x) = \frac{1}{2\gamma} exp((x^2)^\gamma) \frac{x}{(x^2)^\gamma}$ is the predefined-time stabilizing function satisfying $0 < \gamma \le \frac{1}{2}$, ε is a positive parameter.

3.2 Control Law Design

Based on the predefined-time observer, the control laws and adaptive laws are presented as follows:

$$\dot{\boldsymbol{p}}_{id} = -\frac{1}{T_c}\Phi(\boldsymbol{e}_{ip}) - \boldsymbol{e}_{ip} - \hat{P}_i \frac{\boldsymbol{e}_{ip}}{\sqrt{\boldsymbol{e}_{ip}^{\mathrm{T}}\boldsymbol{e}_{ip} + \varepsilon_p^2}} \tag{31}$$

$$\dot{\hat{P}}_i = \beta_{i1}\left(\frac{\boldsymbol{e}_{ip}^{\mathrm{T}}\boldsymbol{e}_{ip}}{\sqrt{\boldsymbol{e}_{ip}^{\mathrm{T}}\boldsymbol{e}_{ip} + \varepsilon_p^2}} - \beta_{i2}\hat{P}_i\right) \tag{32}$$

$$\tilde{\boldsymbol{v}}_i = m_i R_i^{\mathrm{T}} \hat{\vartheta}_i \tilde{\boldsymbol{v}}_{im} \tag{33}$$

$$\tilde{\boldsymbol{v}}_{im} = -\frac{1}{T_c}\Phi(\boldsymbol{e}_{iv}) - \boldsymbol{e}_{iv} - \boldsymbol{\alpha}_i - \hat{\Delta}_i + \ddot{\boldsymbol{p}}_{id} \tag{34}$$

$$\dot{\hat{\vartheta}}_i = \beta_{i3}\left(-\boldsymbol{e}_{iv}^{\mathrm{T}}\tilde{\boldsymbol{v}}_{im} - \beta_{i4}\hat{\vartheta}_i\right) \tag{35}$$

where, $\beta_{i1}, \beta_{i2}, \beta_{i3}, \beta_{i4}, \varepsilon_p$ are controller parameter, $\hat{P}_i, \hat{\vartheta}_i$ are adaptive variable satisfying $\tilde{P}_i = \bar{P}_i - \hat{P}_i$,

$\tilde{\vartheta}_i = \vartheta_i - \hat{\vartheta}_i$, $\tilde{P}_i, \tilde{\vartheta}_i$ denote the corresponding adaptive estimation errors, and $\vartheta_i = \frac{1}{\varsigma_i \sigma} \le \frac{1}{\varsigma_m \sigma} = \bar{\vartheta}_i$.

3.3 Stability analysis

Theorem 1: Under the proposed predefined-time observer(28)-(30), the observation errors $\tilde{\Delta}_i = \Delta_i - \hat{\Delta}_i$ converge to zero within the predefined time T_{c1}.

Proof: Consider the Lyapunov function

$$V_{\Delta} = \tilde{\boldsymbol{e}}_{\Delta}^{\mathrm{T}} \tilde{\boldsymbol{e}}_{\Delta} \tag{36}$$

The time derivative of V_{Δ} gives

$$\begin{aligned} \dot{V}_{\Delta} &= 2\tilde{\boldsymbol{e}}_{\Delta}^{\mathrm{T}} \dot{\tilde{\boldsymbol{e}}}_{\Delta} \\ &= -\frac{2}{T_{c1}} \tilde{\boldsymbol{e}}_{\Delta}^{\mathrm{T}} \Phi(\tilde{\boldsymbol{e}}_{\Delta}) \\ &= -\frac{2}{T_{c1}} \tilde{\boldsymbol{e}}_{\Delta}^{\mathrm{T}} \frac{1}{2\gamma} exp((\tilde{\boldsymbol{e}}_{\Delta}^{\mathrm{T}} \tilde{\boldsymbol{e}}_{\Delta}^{\mathrm{T}})^{\lambda}) \frac{\tilde{\boldsymbol{e}}_{\Delta}}{(\tilde{\boldsymbol{e}}_{\Delta}^{\mathrm{T}} \tilde{\boldsymbol{e}}_{\Delta}^{\mathrm{T}})^{\lambda}} \\ &\le -\frac{1}{\gamma T_{c1}} exp(V_{\Delta}^{\lambda}) V_{\Delta}^{1-\lambda} \end{aligned} \tag{37}$$

According to Lemma 3, $\tilde{\boldsymbol{e}}_{\Delta}$ is guaranteed to converge to zero within the predefined time T_{c1}.Then, it follows that

$$\begin{aligned} \tilde{\Delta}_i &= \Delta_i - \varepsilon \hat{\boldsymbol{e}}_{\Delta} - \dot{\boldsymbol{p}}_{i2} + \dot{\hat{\boldsymbol{p}}}_{i2} \\ &= \Delta_i - \varepsilon \hat{\boldsymbol{e}}_{\Delta} - (\frac{\boldsymbol{R}_i}{m_i} \varsigma_i \sigma \tilde{v}_i + \boldsymbol{\alpha}_i + \Delta_i) + \frac{\boldsymbol{R}_i}{m_i} \varsigma_i \sigma \tilde{v}_i + \boldsymbol{\alpha}_i + \varepsilon \boldsymbol{e}_{\Delta} \\ &= \varepsilon \tilde{\boldsymbol{e}}_{\Delta} \end{aligned} \tag{38}$$

Therefore, $\tilde{\Delta}_i$ also converges to zero within the predefined time T_{c1}.

Theorem 2: Considering the model (18)with input saturations and faults, if choose the control laws and update laws in (31)-(35), the errors defined in (26) and (27) will converge to a bounded set within a predefined time.

Proof: First, the boundedness of the system states is established. Considering the position-loop subsystem, the following Lyapunov function candidate is selected:

$$V_1 = \frac{1}{2} \boldsymbol{e}_p^{\mathrm{T}} \boldsymbol{e}_p + \sum_{i=1}^{n} \frac{\tilde{P}_i^2}{2\beta_{i1}} \tag{39}$$

where $\tilde{P}_i = \bar{P}_i - \hat{P}_i$ is the estimation error, and $\hat{P}_i$ is the estimated value of $\bar{P}_i$.

The time derivative of V_1 gives

$$\begin{aligned} \dot{V}_1 &= \sum_{i=1}^{n} \boldsymbol{e}_{ip}^{\mathrm{T}} (\boldsymbol{e}_{iv} + \dot{\boldsymbol{p}}_{id} - \dot{\boldsymbol{p}}_i^*(t)) - \tilde{P}_i \frac{\boldsymbol{e}_{ip}^{\mathrm{T}} \boldsymbol{e}_{ip}}{\sqrt{\boldsymbol{e}_{ip}^{\mathrm{T}} \boldsymbol{e}_{ip} + \varepsilon_p^2}} + \beta_{i2} \tilde{P}_i \hat{P}_i \\ &= \sum_{i=1}^{n} \boldsymbol{e}_{ip}^{\mathrm{T}} \boldsymbol{e}_{iv} - \frac{1}{T_c} \boldsymbol{e}_{ip}^{\mathrm{T}} \Phi(\boldsymbol{e}_{ip}) - \boldsymbol{e}_{ip}^{\mathrm{T}} \boldsymbol{e}_{ip} - \boldsymbol{e}_{ip}^{\mathrm{T}} \dot{\boldsymbol{p}}_i^*(t) - \hat{P}_i \frac{\boldsymbol{e}_{ip}^{\mathrm{T}} \boldsymbol{e}_{ip}}{\sqrt{\boldsymbol{e}_{ip}^{\mathrm{T}} \boldsymbol{e}_{ip} + \varepsilon_p^2}} - \tilde{P}_i \frac{\boldsymbol{e}_{ip}^{\mathrm{T}} \boldsymbol{e}_{ip}}{\sqrt{\boldsymbol{e}_{ip}^{\mathrm{T}} \boldsymbol{e}_{ip} + \varepsilon_p^2}} + \beta_{i2} \tilde{P}_i \hat{P}_i \\ &\le \sum_{i=1}^{n} -\frac{1}{2} \boldsymbol{e}_{ip}^{\mathrm{T}} \boldsymbol{e}_{ip} - \frac{1}{T_c} \boldsymbol{e}_{ip}^{\mathrm{T}} \Phi(\boldsymbol{e}_{ip}) + \left\| \boldsymbol{e}_{ip}^{\mathrm{T}} \right\| \bar{P}_i - \bar{P}_i \frac{\boldsymbol{e}_{ip}^{\mathrm{T}} \boldsymbol{e}_{ip}}{\sqrt{\boldsymbol{e}_{ip}^{\mathrm{T}} \boldsymbol{e}_{ip} + \varepsilon_p^2}} + \beta_{i2} \tilde{P}_i \hat{P}_i + \frac{1}{2} \boldsymbol{e}_{iv}^{\mathrm{T}} \boldsymbol{e}_{iv} \\ &\le \sum_{i=1}^{n} -\frac{1}{2} \boldsymbol{e}_{ip}^{\mathrm{T}} \boldsymbol{e}_{ip} - \frac{1}{T_c} \boldsymbol{e}_{ip}^{\mathrm{T}} \Phi(\boldsymbol{e}_{ip}) - \frac{\beta_{i2}}{2} \tilde{P}_i^2 + \bar{P}_i \varepsilon_p + \frac{\beta_{i2}}{2} \bar{P}_i^2 + \frac{1}{2} \boldsymbol{e}_{iv}^{\mathrm{T}} \boldsymbol{e}_{iv} \end{aligned} \tag{40}$$

For the velocity-loop subsystem, consider the following Lyapunov function candidate:

$$V_2 = \frac{1}{2} \boldsymbol{e}_v^{\mathrm{T}} \boldsymbol{e}_v + \sum_{i=1}^{n} \frac{\varsigma_m \sigma \tilde{\vartheta}_i^2}{2\beta_{i3}} \tag{41}$$

The time derivative of V_2 gives

$$
\begin{aligned}
\dot{V}_2 &= \sum_{i=1}^{n} \boldsymbol{e}_{iv}^{\mathrm{T}}\left(\frac{\boldsymbol{R}_i}{m_i}\varsigma_i\sigma\tilde{\boldsymbol{v}}_i + \boldsymbol{\Delta}_i + \boldsymbol{\alpha}_i - \dot{\boldsymbol{p}}_{i2d}\right) - \varsigma_m\sigma\tilde{\vartheta}_i\left(-\boldsymbol{e}_{iv}^{\mathrm{T}}\tilde{v}_{im} - \beta_{i6}\hat{\vartheta}_i\right) \\
&= \sum_{i=1}^{n} \boldsymbol{e}_{iv}^{\mathrm{T}}\left(-\frac{1}{T_c}\Phi(\boldsymbol{e}_{iv}) - \boldsymbol{e}_{iv} - \boldsymbol{\alpha}_i - \hat{\boldsymbol{\Delta}}_i + \boldsymbol{\Delta}_i + \boldsymbol{\alpha}_i\right) + \varsigma_m\sigma\beta_{i4}\tilde{\vartheta}_i\hat{\vartheta}_i \\
&= \sum_{i=1}^{n} \boldsymbol{e}_{iv}^{\mathrm{T}}\left(-\frac{1}{T_c}\Phi(\boldsymbol{e}_{iv}) - \boldsymbol{e}_{iv} + \tilde{\boldsymbol{\Delta}}_i\right) + \varsigma_m\sigma\beta_{i4}\tilde{\vartheta}_i\hat{\vartheta}_i \\
&= \sum_{i=1}^{n} \boldsymbol{e}_{iv}^{\mathrm{T}}\left(-\frac{1}{T_c}\Phi(\boldsymbol{e}_{iv}) - \boldsymbol{e}_{iv} + \tilde{\boldsymbol{\Delta}}_i\right) + \varsigma_m\sigma\beta_{i4}\tilde{\vartheta}_i\left(\vartheta_i - \tilde{\vartheta}_i\right) \\
&\le \sum_{i=1}^{n} -\frac{1}{T_c}\boldsymbol{e}_{iv}^{\mathrm{T}}\Phi(\boldsymbol{e}_{iv}) - \frac{1}{2}\boldsymbol{e}_{iv}^{\mathrm{T}}\boldsymbol{e}_{iv} + \frac{1}{2}\tilde{\boldsymbol{\Delta}}_i^{T}\tilde{\boldsymbol{\Delta}}_i - \frac{1}{2}\varsigma_m\sigma\beta_{i4}\tilde{\vartheta}_i^2 + \frac{1}{2}\varsigma_m\sigma\beta_{i4}\vartheta_i^2
\end{aligned}
\tag{42}
$$

Consider the Lyapunov function

$$
V = V_1 + V_2 \tag{43}
$$

The time derivative of V gives

$$
\begin{aligned}
\dot{V} &= \dot{V}_1 + \dot{V}_2 \\
&= \sum_{i=1}^{n} -\frac{1}{2}\boldsymbol{e}_{ip}^{\mathrm{T}}\boldsymbol{e}_{ip} - \frac{1}{T_c}\boldsymbol{e}_{ip}^{\mathrm{T}}\Phi(\boldsymbol{e}_{ip}) - \frac{\beta_{i2}}{2}\tilde{P}_i^2 + \bar{P}_i\varepsilon_p + \frac{\beta_{i2}}{2}\bar{P}_i^2 + \frac{1}{2}\boldsymbol{e}_{iv}^{\mathrm{T}}\boldsymbol{e}_{iv} - \frac{1}{T_c}\boldsymbol{e}_{iv}^{\mathrm{T}}\Phi(\boldsymbol{e}_{iv}) - \\
&\frac{1}{2}\boldsymbol{e}_{iv}^{\mathrm{T}}\boldsymbol{e}_{iv} + \frac{1}{2}\tilde{\boldsymbol{\Delta}}_i^{T}\tilde{\boldsymbol{\Delta}}_i - \frac{1}{2}\varsigma_m\sigma\beta_{i4}\tilde{\vartheta}_i^2 + \frac{1}{2}\varsigma_m\sigma\beta_{i4}\vartheta_i^2 \\
&\le \sum_{i=1}^{n} -\frac{1}{2}\boldsymbol{e}_{ip}^{\mathrm{T}}\boldsymbol{e}_{ip} - \frac{1}{T_c}\boldsymbol{e}_{ip}^{\mathrm{T}}\Phi(\boldsymbol{e}_{ip}) - \frac{\beta_{i2}}{2}\tilde{P}_i^2 - \frac{1}{T_c}\boldsymbol{e}_{iv}^{\mathrm{T}}\Phi(\boldsymbol{e}_{iv}) - \frac{1}{2}\varsigma_m\sigma\beta_{i4}\tilde{\vartheta}_i^2 + \bar{P}_i\varepsilon_p + \frac{\beta_{i2}}{2}\bar{P}_i^2 + \\
&\frac{1}{2}\tilde{\boldsymbol{\Delta}}_i^{T}\tilde{\boldsymbol{\Delta}}_i + \frac{1}{2}\varsigma_m\sigma\beta_{i4}\vartheta_i^2 \\
&\le \sum_{i=1}^{n} -\left(\frac{1}{2} + \frac{1}{2\gamma T_c}\right)\boldsymbol{e}_{ip}^{\mathrm{T}}\boldsymbol{e}_{ip} - \frac{\beta_{i2}}{2}\tilde{P}_i^2 - \frac{1}{2\gamma T_c}\boldsymbol{e}_{iv}^{\mathrm{T}}\boldsymbol{e}_{iv} - \frac{\varsigma_m\sigma\beta_{i4}}{2}\tilde{\vartheta}_i^2 + \bar{P}_i\varepsilon_p + \frac{\beta_{i2}}{2}\bar{P}_i^2 + \\
&\frac{1}{2}\tilde{\boldsymbol{\Delta}}_i^{T}\tilde{\boldsymbol{\Delta}}_i + \frac{1}{2}\beta_{i4}\bar{\vartheta}_i^2 \\
&\le -\mu V + \delta
\end{aligned}
\tag{44}
$$

where $\mu = min\{\dfrac{\frac{1}{2} + \frac{1}{2\gamma T_c}}{\lambda_{max}\left(\bar{\boldsymbol{\Omega}}_{ff}^{-1}\right)}, \dfrac{1}{2\gamma T_c}, \dfrac{\beta_{i2}}{2}, \dfrac{\beta_{i4}}{2}\}$, $\delta = \bar{P}_i\varepsilon_p + \dfrac{\beta_{i2}}{2}\bar{P}_i^2 + \dfrac{\beta_{i4}}{2}\bar{\vartheta}_i^2$. From (44), it can be concluded that all elements of the system state vector $E = \left\{\boldsymbol{e}_{ip}, \boldsymbol{e}_{iv}, \tilde{P}_i, \tilde{\vartheta}_i\right\}$ are uniformly ultimately bounded after T_{c1}.

Next, to establish the predefined -time convergence of the closed-loop system, the following Lyapunov function candidate is selected:

$$
V_t = \boldsymbol{e}_p^{\mathrm{T}}\boldsymbol{e}_p + \boldsymbol{e}_v^{\mathrm{T}}\boldsymbol{e}_v \tag{45}
$$

The time derivative of V_t gives

$$
\begin{aligned}
\dot{V}_t &= 2\sum_{i=1}^{n} \boldsymbol{e}_{ip}^{\mathrm{T}}(\dot{\boldsymbol{p}}_i(t)-\dot{\boldsymbol{p}}_i^{*}(t))+\boldsymbol{e}_{iv}^{\mathrm{T}}(\ddot{\boldsymbol{p}}_i(t)-\ddot{\boldsymbol{p}}_{id}(t)) \\
&= 2\sum_{i=1}^{n} \boldsymbol{e}_{ip}^{\mathrm{T}}\boldsymbol{e}_{iv}-\frac{1}{T_c}\boldsymbol{e}_{ip}^{\mathrm{T}}\Phi(\boldsymbol{e}_{ip})-\boldsymbol{e}_{ip}^{\mathrm{T}}\boldsymbol{e}_{ip}+ \\
&\quad \boldsymbol{e}_{iv}^{\mathrm{T}}(\varsigma_i\sigma\hat{\vartheta}_i\tilde{\boldsymbol{v}}_{im}+\Delta_i+\boldsymbol{\alpha}_i)- \\
&\quad \hat{P}_i\frac{\boldsymbol{e}_{ip}^{\mathrm{T}}\boldsymbol{e}_{ip}}{\sqrt{\boldsymbol{e}_{ip}^{\mathrm{T}}\boldsymbol{e}_{ip}+\varepsilon_p^2}}-\boldsymbol{e}_{ip}^{\mathrm{T}}\dot{\boldsymbol{p}}_i^{*}(t) \\
&\le 2\sum_{i=1}^{n} -\frac{1}{T_c}\boldsymbol{e}_{ip}^{\mathrm{T}}\Phi(\boldsymbol{e}_{ip})-\frac{1}{T_c}\boldsymbol{e}_{iv}^{\mathrm{T}}\Phi(\boldsymbol{e}_{iv})+\hat{P}_i\varepsilon_p+ \\
&\quad \frac{\left\|\tilde{\vartheta}_i\right\|^2\left\|\tilde{\boldsymbol{v}}_{im}\right\|^2}{2}+\frac{\left\|\tilde{P}_i\right\|^2}{2}
\end{aligned}
\tag{46}
$$

Since all elements of the system state vector $E=\left\{\boldsymbol{e}_{ip},\boldsymbol{e}_{iv},\tilde{P}_i,\tilde{\vartheta}_i\right\}$ are uniformly ultimately bounded, $\tilde{\boldsymbol{v}}_{im}$ is bounded. By Lemmas 4 and 5, it follows that

$$
\begin{aligned}
&-\frac{2}{T_c}\boldsymbol{e}_{ip}^{\mathrm{T}}\Phi(\boldsymbol{e}_{ip})-\frac{2}{T_c}\boldsymbol{e}_{iv}^{\mathrm{T}}\Phi(\boldsymbol{e}_{iv}) \\
&=-\frac{2}{T_c}\boldsymbol{e}_{ip}^{\mathrm{T}}\frac{1}{2\gamma}exp((\boldsymbol{e}_{ip}^2)^{\lambda})\frac{\boldsymbol{e}_{ip}}{(\boldsymbol{e}_{ip}^{T}\boldsymbol{e}_{ip})^{\lambda}}- \\
&\frac{2}{T_c}\boldsymbol{e}_{iv}^{\mathrm{T}}\frac{1}{2\gamma}exp((\boldsymbol{e}_{iv}^2)^{\lambda})\frac{\boldsymbol{e}_{iv}}{(\boldsymbol{e}_{iv}^{T}\boldsymbol{e}_{iv})^{\lambda}} \\
&\le -\frac{1}{\gamma T_c}\left[exp\left(\frac{1}{2}(V)^{\lambda}\right)\right][V]^{1-\lambda}
\end{aligned}
\tag{47}
$$

Thus,

$$
\dot{V}_t \le -\frac{1}{\gamma T_c}\left[exp\left(\frac{1}{2}(V_t)^{\lambda}\right)\right][V_t]^{1-\lambda}+\delta_t \tag{48}
$$

Where $\delta_t=\sum_{i=1}^{n}2\hat{P}_i\varepsilon_p+\left\|\tilde{P}_i\right\|^2+\hat{D}\varepsilon_v+\left\|\tilde{\vartheta}_i\right\|^2\left\|\tilde{\boldsymbol{v}}_{im}\right\|^2$. According to Lemma 2, the system error converges to the neighborhood $\Omega=min\{\Omega_1,\Omega_2\}$ within the prescribed time $t=T_{c1}+max\{t_1,t_2\}$, where

$$
\begin{cases}
t_1=\dfrac{2T_c}{\alpha}(1-exp(-\dfrac{1}{2}V_t^{\gamma}(0)))<\dfrac{2T_c}{\alpha} \\
t_2=\dfrac{2T_c}{(1-\alpha)}(1-exp(-\dfrac{1}{2}V_t^{\gamma}(0)))<\dfrac{2T_c}{(1-\alpha)}
\end{cases}
\tag{49}
$$

$$
\begin{cases}
\Omega_1=\left\{\boldsymbol{e}_{ip},\boldsymbol{e}_{iv}\left|exp(\dfrac{1}{2}V_t^{\gamma})V_t^{1-\gamma}\le\dfrac{\delta_t\gamma T_c}{1-\alpha}\right.\right\} \\
\Omega_2=\left\{\boldsymbol{e}_{ip},\boldsymbol{e}_{iv}\left|exp(\dfrac{1}{2}V_t^{\gamma})V_t^{1-\gamma}\le\dfrac{\delta_t\gamma T_c}{\alpha}\right.\right\}
\end{cases}
\tag{50}
$$

4. Simulation results

In this subsection, a simulation scenario is designed to verify the performance of the predefined-time fault-tolerant affine formation control strategy for multi-UAV systems with input magnitude constraints. Consider a UAV team consisting of four followers and three leaders. The velocities of leaders are designed as $V_l=25\mathrm{m/s}$. It is assumed that all leader UAVs are capable of tracking their desired trajectories without faults, and their movements are pre-designed. The initial states of UAVs are shown in Table 1. The parameters of the observer and control system are shown in Table 2. Moreover, the mass of the UAV is chosen as 5 kg and the disturbance is defined as

$\boldsymbol{d}_{i0} = \left[sin(t), 0.5(cos(0.8t) + sin(0.4t + 0.2)), 0.1(sin(t) + cos(t))\right]^{\mathrm{T}} m/s^2$. The followers' input magnitude bounds are chosen as $\bar{u}_x = 150N$, $\bar{u}_y = -\underline{u}_y = 60N$, $\bar{u}_z = -\underline{u}_z = 60N$, and $\underline{u}_x = 0N$. To illustrate the fault-tolerant performance of the control strategy, actuator faults are introduced for the followers, as detailed in Table 3.

Table 1 Initial states of UAVs.

	$\boldsymbol{p}_{i1}(0)/m$	$\boldsymbol{p}_{i2}(0)/(m/s)$
Leader 1	$[5, 0, 100]^{\mathrm{T}}$	$[25, 0, 0]^{\mathrm{T}}$
Leader 2	$[0, 5, 100]^{\mathrm{T}}$	$[25, 0, 0]^{\mathrm{T}}$
Leader 3	$[0, -5, 100]^{\mathrm{T}}$	$[25, 0, 0]^{\mathrm{T}}$
Follower 1	$[-4, -4, 100]^{\mathrm{T}}$	$[20, 0, 0]^{\mathrm{T}}$
Follower 2	$[-5, -6, 100]^{\mathrm{T}}$	$[20, 0, 0]^{\mathrm{T}}$
Follower 3	$[-10, 5, 100]^{\mathrm{T}}$	$[20, 0, 0]^{\mathrm{T}}$
Follower 4	$[-9, -5, 100]^{\mathrm{T}}$	$[20, 0, 0]^{\mathrm{T}}$

Table 2 Parameters of control system.

Parameters	Values
$T_{c1}, \varepsilon, \sigma$	4, 0.35,1
$T_c, \varepsilon_P, \beta_{i1}, \beta_{i2}, \beta_{i3}, \beta_{i4}$	4, 0.8, 0.05, 0.5,0.1,0.5

Table 3 Faults information.

UAV	Time	$\varsigma_i(t)$	$\boldsymbol{h}_i(t)$
Follower 1	15s	$diag\{0.9 + 0.1exp(-2max\{0, t - t_{fault}\}), 1, 1\}$	$\left[-5(1 - exp(-2max\{0, t - t_{fault}\})), 0, 0\right]^{\mathrm{T}}$
Follower 2	30s	$diag\{1, 0.6 + 0.4exp(-2max\{0, t - t_{fault}\}), 1\}$	$\left[0, 10(1 - exp(-2max\{0, t - t_{fault}\})), 0\right]^{\mathrm{T}}$
Follower 3	50s	$diag\{1, 1, 0.8 + 0.2exp(-2max\{0, t - t_{fault}\})\}$	$\left[0, 0, -1.5(1 - exp(-2max\{0, t - t_{fault}\}))\right]^{\mathrm{T}}$
Follower 4	10s	$diag\{0.7 + 0.3exp(-2max\{0, t - t_{fault}\}), 1, 1\}$	$\left[-5(1 - exp(-2max\{0, t - t_{fault}\})), 0, 0\right]^{\mathrm{T}}$

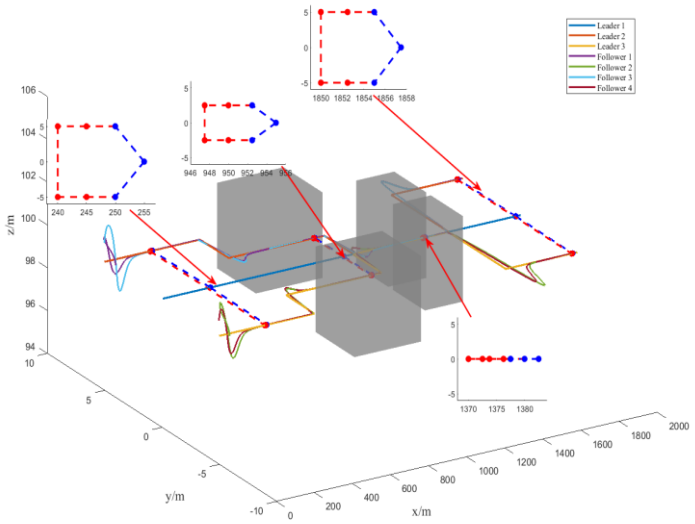
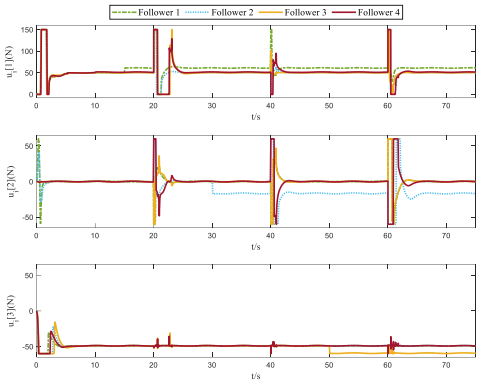
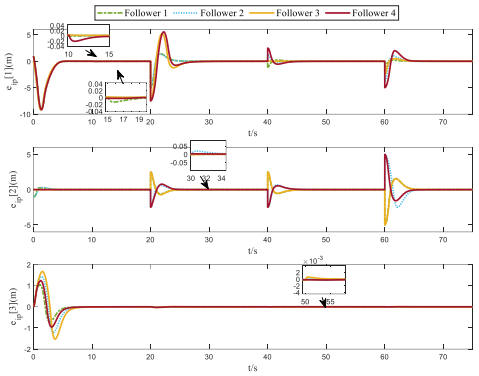


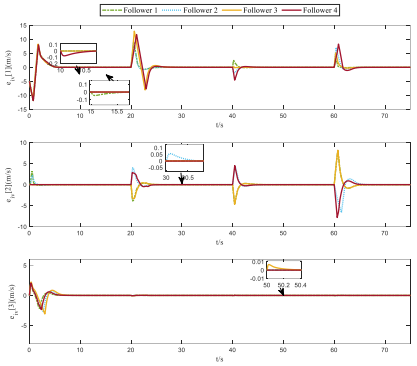
Figure 1 – Three-dimensional trajectory of UAV formations.



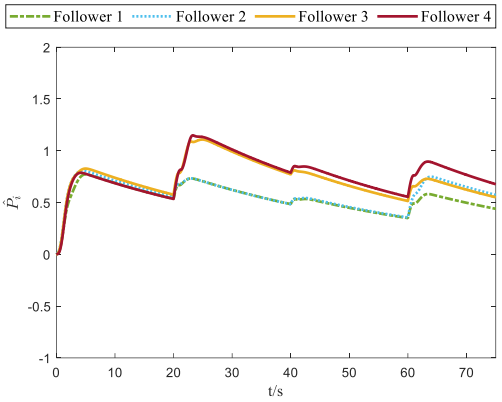
(a) Control input signals of followers.



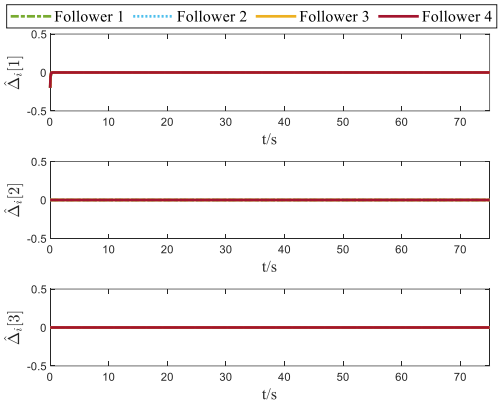
(b) Position errors of followers.



(c) Velocity errors of UAV followers.



(d) Curves of $\hat{P}_i$.



(e) Curves of $\hat{\Delta}_i$.

Figure 2 – Simulation of followers.

The above simulation results demonstrate that, under the proposed control law, the UAV formation composed of three leader UAVs and four follower UAVs successfully achieves maneuvering transformations in complex terrain environments and forms the desired formation. The position and velocity errors of the UAVs are shown in Figure 2 (a) and Figure 2 (b). It can be observed that the position and velocity errors converge to a neighborhood of the origin within the predefined time, and the control inputs of the system shown in Figure 2 (c) satisfy the prescribed constraints. The adaptive signals $\hat{P}_i$ and observer errors are shown in Figure 2 (d) and Figure 2 (e), respectively. It can be observed that the observer errors converge within the predefined time, while the adaptive signals remain bounded throughout the process.

5. Conclusion

This paper proposes a predefined-time fault-tolerant affine formation control law for multi-UAV

systems with input magnitude. Firstly, a novel smooth approximation function is proposed to effectively handle asymmetric control input constraints. Secondly, based on the proposed smooth function and a predefined-time disturbance observer, a predefined-time affine formation fault-tolerant control strategy is developed to simultaneously handle actuator faults, external disturbances, and input constraints. Finally, the simulation results demonstrate that the proposed method can achieve the desired affine formation, including translation and scaling, while guaranteeing predefined-time convergence of the formation errors.

6. Copyright Statement

The authors confirm that they, and/or their company or organization, hold copyright on all of the original material included in this paper. The authors also confirm that they have obtained permission, from the copyright holder of any third party material included in this paper, to publish it as part of their paper. The authors confirm that they give permission, or have obtained permission from the copyright holder of this paper, for the publication and distribution of this paper as part of the ICAS proceedings or as individual off-prints from the proceedings.

References

[1] P. V K. *Advances in unmanned aerial vehicles: state of the art and the road to autonomy* [M]. Springer, 2007.

[2] Chen C, Liu Y, Zhang Y. An enhanced anti-disturbance finite-time exponentially convergent parameter estimator for quadrotor UAVs with unknown uncertain dynamics[J]. *ISA transactions*, Vol. 173: pp 243-257, 2026.

[3] Qiu Z, Zhang L, Chi Y, et al. Active obstacle avoidance of multi-rotor UAV swarm based on stress matrix formation method [J]. *Mathematics*, Vol. 13, No. 1: pp 86, 2025.

[4] Lin Z, Wang L, Chen Z, et al. Necessary and sufficient graphical conditions for affine formation control [J]. *IEEE Transactions on Automatic Control*, Vol. 61, No. 10: pp 2877-2891, 2016.

[5] Zhao S. Affine formation maneuver control of multiagent systems[J]. *IEEE Transactions on Automatic Control*, Vol. 63, No. 12: pp 4140-4155, 2018.

[6] Xu Y, Zhao S, Luo D, et al. Affine formation maneuver control of high-order multi-agent systems over directed networks [J]. *Automatica*, Vol. 118: pp 109004, 2020.

[7] Li H, Chen H, Wang X, et al. Distributed framework construction for affine formation control[J]. *IEEE Transactions on Automatic Control*, Vol. 71, No. 1: pp 243-258, 2026.

[8] Chen L, Mei J, Li C, et al. Distributed leader–follower affine formation maneuver control for high-order multiagent systems[J]. *IEEE Transactions on Automatic Control*, Vol. 65, No. 11, pp 4941-4948, 2020.

[9] Lin Y, Lin Z, Sun Z, et al. A unified approach for finite-time global stabilization of affine, rigid, and translational formation[J]. *IEEE Transactions on Automatic Control*, Vol. 67, No. 4: pp 1869-1881, 2021.

[10] Xu Z, Lan Y, Lei C. Fixed-time disturbance observer-based fixed-time prescribed performance control for nonlinear systems with disturbances and full-state constraints[J]. *International Journal of Control, Automation and Systems*, Vol. 20, No. 10: pp 2999-3007, 2024.

[11] Yang X, Qu Y, DELIN L, et al. Distributed predefined-time estimator-based affine formation target-enclosing maneuver control for cooperative underactuated quadrotor UAVs with fault-tolerant capabilities[J]. *Chinese Journal of Aeronautics*, Vol. 38, No. 1: pp 103042, 2025.

[12] Wang H, Dong J. Neural network-based hierarchical fault-tolerant affine formation control for heterogeneous nonlinear multi-agent systems[J]. *IEEE Transactions on Intelligent Transportation Systems*, Vol. 25, No. 5: pp 4503-4511, 2023.

[13] Zhu G, Du J. Global robust adaptive trajectory tracking control for surface ships under input saturation [J]. *IEEE Journal of Oceanic Engineering*, Vol. 45, No. 2: pp 442-450, 2018.

[14] Yu J, Shi P, Lin C, et al. Adaptive neural command filtering control for nonlinear MIMO systems with saturation input and unknown control direction [J]. *IEEE Transactions on Cybernetics*, Vol. 50, No. 6: pp 2536-2545, 2019.

[15] Ma L, Zong G, Zhao X, et al. Observed-based adaptive finite-time tracking control for a class of nonstrict-feedback nonlinear systems with input saturation [J]. *Journal of the Franklin Institute*, Vol. 357, No. 16: pp 11518-11544, 2020.

[16] Hao Y, Fang Z, Cao J, et al. Consensus control of nonlinear fractional-order multiagent systems with input saturation: a t-s fuzzy method [J]. *IEEE Transactions on Fuzzy Systems,* Vol. 32, No. 12: pp 6754-6766, 2024.

[17] Zhu G, Du J. Robust adaptive neural practical fixed-time tracking control for uncertain Euler-Lagrange systems under input saturations [J]. *Neurocomputing*, Vol. 412: pp 502-513, 2020.

[18]Sun Y, Lyu Y, Guo Y, et al. Adaptive predefined-time control for liquid-filled flexible spacecraft attitude stabilization during orbit maneuver [J]. *Advances in Space Research*, Vol. 71, No. 6: pp 2733-2744, 2023.

[19]Zuo Z, Wang C. Adaptive trajectory tracking control of output constrained multi-rotors systems [J]. IET Control Theory & Applications, Vol. 8, No. 13: pp 1163-1174, 2014.

[20]Jiménez-Rodríguez E, Sánchez-Torres J D, Loukianov A G. Predefined-time backstepping control for tracking a class of mechanical systems [J]. *IFAC-PapersOnLine*, Vol. 20, No. 1: pp 1680-1685, 2017.